Tellus (1995), 47A, 849–863
Printed in Belgium – all rights reserved

TELLUS
ISSN 0280–6495

Stratosphere-troposphere interactions associated with a case of explosive cyclogenesis in the Labrador Sea

By M. CATHERINE READER and G. W. KENT MOORE*, *Department of Physics, University of Toronto, Toronto, Ontario, Canada M5S 1A7*

(Manuscript received 29 August 1994; in final form 18 April 1995)

ABSTRACT

There is considerable evidence that many extra-tropical cyclones are generated by the interaction between an upper-level potential vorticity anomaly and a low-level baroclinic zone. A variety of satellite data and the ECMWF high-resolution objectively-analyzed fields are used to investigate the origin of these tropopause features and their role in cyclogenesis for a remarkable rapidly developing cyclone that developed in the Labrador Sea on 1 and 2 March 1992. According to the ECMWF analysis, this storm deepened by 42 mb in 24 h, attaining a central pressure of less than 935 mb on 2 March. The use of satellite column ozone data, from the TOMS and TOVS instruments is emphasized for the identification of mesoscale tropopause features implicated in cyclogenesis. Both data sets are able to resolve the intrusions of ozone-rich stratospheric air associated with this storm.

1. Introduction

The idea that upper-level vortices can induce cyclogenesis in a surface baroclinic region was introduced by Kleinschmidt over 40 years ago (Kleinschmidt 1950a, 1950b, 1951). Since then, considerable observational evidence has been amassed that demonstrates the importance of this mechanism, termed "Type B cyclogenesis" by Petterssen and Smebye (1971), in the triggering of certain types of cyclones (see also, for example, Bleck, 1973). This idea has been further developed by Uccellini et al., 1985 and Whitaker, 1988. Uccellini, 1990 provides a comprehensive treatment of the role of upper-level vortices in cyclogenesis.

The potential vorticity and potential temperature fields provide an excellent framework for the investigation of upper-level involvement in cyclogenesis (see, e.g., Hoskins et al., 1985). Ertel's potential vorticity,

$$\mathrm{PV} = \rho^{-1} \xi_a \cdot \nabla\theta \qquad (1)$$

(where θ is the potential temperature and ξ_a is the absolute vorticity), is an extremely useful quantity for the study of the role that upper-level processes play in cyclogenesis because, in the absence of diabatic effects, it is materially conserved. Isentropic potential vorticity (IPV), i.e., PV expressed in isentropic coordinates

$$\mathrm{IPV} = -g(f + \boldsymbol{k} \cdot \nabla_\theta \times \boldsymbol{v})/(\partial p/\partial\theta), \qquad (2)$$

(where the hydrostatic approximation and the usual meteorological practice of neglecting horizontal terms in the gradient have also been applied), is conserved on isentropic surfaces under these circumstances, as well. PV and IPV can therefore serve as approximate air-mass tracers. In particular, since stratospheric values of potential vorticity are typically much higher than those in the troposphere (because of the steep static stability gradient), PV and IPV are useful indicators of air of recent stratospheric origin (Danielson, 1968). In fact, the 2 PVU (1 PVU = 10^{-6} K Pa^{-1} m s^{-3}) contour provides a good working definition of the tropopause at mid-latitudes (Thorncroft et al., 1993).

* Corresponding author.

An important consequence of IPV conservation for this work, is, roughly speaking, the interchangeability of vorticity and potential temperature gradient. When stratospheric air intrudes adiabatically into the troposphere the isentropic surfaces are vertically spread apart within the intrusion. As a result, the denominator, $(\partial p/\partial\theta)$, of eq. (2) increases within the anomaly. To conserve IPV the cyclonic circulation must therefore increase as well.

According to the Type B cyclogenesis scenario, such an upper-level vortex can, under suitable conditions, induce a low-level circulation. When an upper-level PV anomaly approaches a surface baroclinic region (or pre-existing PV or temperature anomaly) the cyclonic flow associated with the upper vortex induces (or enhances) the surface anomaly just ahead of it which, in turn, generates a reinforcing circulation. This reinforcing process can occur as long as the upper vortex is upstream from the surface anomaly. An excellent review of this mechanism is provided in Hoskins et al. (1985). The effectiveness of this mechanism for triggering cyclogenesis has been shown in a simplified model study as well (Takayabu, 1991).

Stratospheric PV anomalies can also be identified in column ozone data. As originally recognized by Reed (1950), the descent of ozone-rich stratospheric air requires convergence in the lower stratosphere, resulting in a local increase in the total column amount. Two sources of satellite ozone data, TOMS and TOVS, are examined in this case study.

Section 2 is a description of a cyclone that underwent rapid development in the Labrador Sea during the Canadian Atlantic Storms Project II (CASP II). Section 3 outlines the various data sets used in this study. Section 4 relates a scenario for the evolution of this storm that is suggested by the above data. Of particular significance is that the upper-level PV anomaly which seems to have been important in the development of this cyclone appears to have been part of a train of PV anomalies along the polar front. This coherent structure is also apparent in TOVS column ozone data, some of whose advantages and disadvan-

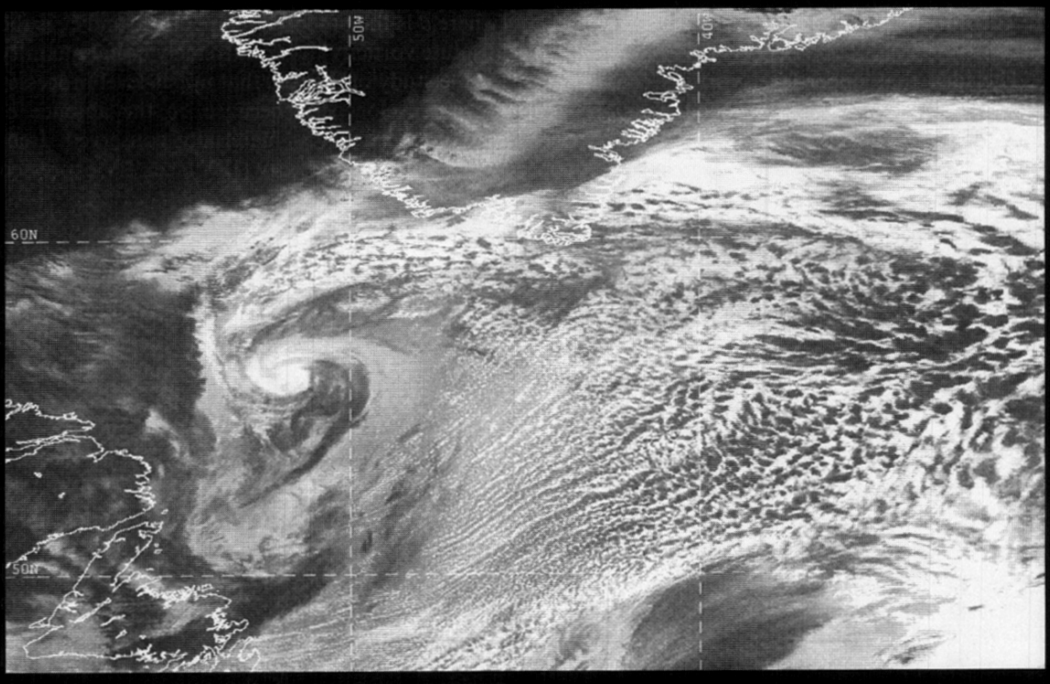

Fig. 1. An AVHRR channel 4 infrared image of the cyclone on 17:06 GMT, 2 March 1992.

tages are complementary to the more frequently studied TOMS data. Finally, we summarize our conclusions in Section 5.

2. Case description

The 2 March 1992 case of explosive cyclogenesis which occurred in the Labrador Sea during the Canadian Atlantic Storms Project II (CASP II), presents us with an ideal situation for shedding light on various processes involved in extra-tropical cyclogenesis. The dramatic nature of this storm, combined with the large amount of data available, yields an exceptionally clear picture of the role of upper-level features in its development.

This cyclone was characterized by an extremely rapid pressure drop and low minimum central pressure. Fig. 1 is an infrared AVHRR image of this storm on 2 March 1992 at 17:06 GMT, shortly after it reached maximum depth. Note the somewhat complicated and asymmetrical cloud field associated with the cyclone and its very prominent eye at approximately 56°N, 52°W. The many streamers indicate the flow of cold continental air over the Labrador Sea, associated with the storm, and the resulting surface heat flux and convection.

This remarkable central pressure drop, 42 mb in 24 h, is evident in the European Centre for Medium-Range Weather Forecasting (ECMWF) objective analysis. Fig. 2 is a graph of the time-evolution of the minimum surface pressure for this system from 00:00 GMT on 28 February to 06:00 GMT on 3 March 1992, according to the ECMWF data. It shows the period of gradual deepening as the low tracked across the continent on 28 and 29 February, followed by the 24-h period of explosive development in the Labrador Sea, beginning around 00 GMT on 1 March. The maximum depth, less than 935 mb, was reached at approximately 00 GMT on 2 March, at which time it began to fill rapidly.

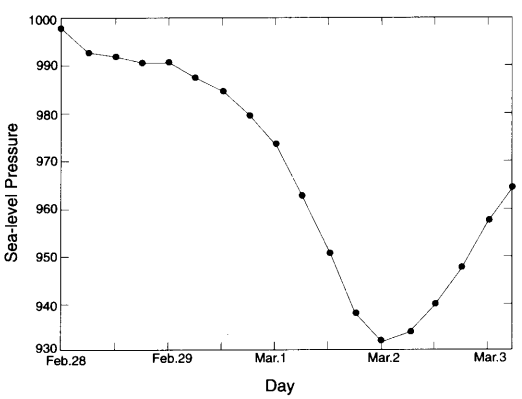

Fig. 2. The time evolution of the central pressure of the surface low showing the long period of slow growth followed by the explosive deepening and rapid filling of the storm.

This storm is notable in that it underwent explosive deepening near the sea ice edge in the Labrador Sea, well North of the well-studied "bomb centre" along the Gulf Stream (Sanders and Gyakum, 1980; Sanders, 1980; Roebber, 1984). There are, however, other documented cases of explosive cyclogenesis in this region (Reed et al., 1988). Like the above-mentioned Gulf Stream bombs, the ECMWF analysis suggests that pre-existing upper-level potential-vorticity anomalies played a crucial role in the development of this storm. This upper-level structure is also reflected in column ozone data; the lower tropopause associated with a PV anomaly implies an influx of ozone-rich stratospheric air, resulting in locally increased total ozone measurements.

3. Description of data

3.1. The analyzed fields

The 6-hourly high-resolution objectively analyzed fields used in this study are from the European Centre for Medium-Range Weather Forecasting (ECMWF) level III data set (ECMWF, 1992). This data is on a 1.125° Gaussian grid, interpolated to a rectangular grid. The upper-level fields have 15 vertical pressure levels between 1000 mb and 10 mb. The relatively long (up to 18 h) data collection cutoff time used for generating the ECMWF fields is an advantage for studies like this one, since it allows inclusion of data from remote stations. In this work, we examine the sea-level pressure field, temperature, geopotential height, relative humidity and horizontal wind fields as well as several quantities derived from these fields using the GEMPAK software package developed at the National Meteorological Center (NMC) and distributed by the National Center for Atmospheric Research (NCAR).

We calculate approximations to potential vor-

ticity from the standard fields by replacing the derivatives by finite differences between pressure levels, applying the hydrostatic approximation and neglecting the horizontal terms in the potential temperature gradient, i.e.:

$$\overline{\mathrm{PV}} = -g\bar{\xi}_a\left(\frac{\Delta\theta}{\Delta P}\right), \tag{3}$$

where $\bar{\xi}_a$ is that average vorticity of the two bounding layers and $\Delta\theta$ and ΔP are the potential temperature and pressure differences between the layers, respectively. We also interpolate the pressure-level data to isentropic levels.

We present maps of 500 mb–1000 mb thickness as well. This quantity is related to the temperature, averaged with respect to the logarithm of the pressure, via the ideal gas law.

3.2. The satellite data

The satellite images presented here are Advanced Very High Resolution Radiometer (AVHRR) channel 4 (10.8 μm) infrared images from the NOAA 11 and NOAA 12 polar-orbitting satellites. The images are ingested, registered and enhanced using the Terascan software package and printed in the negative, so that dark areas indicate high radiance (i.e., high brightness temperatures).

TOMS satellite column ozone data has been used successfully as a qualitative indicator of tropopause structure in a number of meteorological phenomena, including jets (Shapiro et al., 1982; Sechrist et al., 1986), tropical cyclones (Rodgers et al., 1990), baroclinic waves (Mote et al., 1991) and explosive extratropical cyclones, (Uccellini et al., 1985; Reed and Albright, 1986; Gyakum and Barker, 1988). We examine a complementary source of satellite column ozone data from the TOVS instruments as well as the TOMS data.

The TOVS (TIROS-n Operational Vertical Sounder) instruments, aboard the NOAA series satellites, measure a number of infrared and microwave radiances. We use the International TOVS Processing package, developed at the University of Wisconsin at Madison, to retrieve total column ozone measurements from this data (Smith et al., 1985). An initial guess ozone profile is obtained by linear regression on several infrared radiances, measured by the HIRS (High-resolution Infrared Sounder) radiometer. This guess is then used in a physical retrieval based on the radiative transfer equation for HIRS channel 9, which corresponds to an ozone absorption line. The TOVS data has the advantage of being coincident with the AVHRR images from the NOAA satellites. The TOVS resolution is typically about 80 km near the centre of the pass, though the sounding distribution is not uniform because of the cloud-clearing algorithm.

The TOMS (Total Ozone Mapping Spectrometer) instrument, on the Nimbus-7 platform, measures column ozone using back-scattered ultraviolet radiation. It is a scanning instrument with a resolution of 50 km at nadir and provides daily global coverage. The NASA "GRIDTOMS" product, which contains averages of the total ozone in each grid cell for the ascending orbit closest to nadir, was used in this study. The data has been interpolated to a regular 1.00° latitude by 1.25° longitude grid from the original latitude-dependent grid*. The random error in the TOMS data is thought to be only 2% (McPeters et al., 1993), so in the absence of high levels of volcanic aerosols in the stratosphere, or polar stratospheric clouds, this should indicate the level at which local variations in the TOMS data reflect actual ozone variations (regardless of the absolute accuracy of the data).

4. The storm evolution

4.1. The ECMWF analysis

Figs. 3a, 4a show a series of plots of potential vorticity in the 400 to 500 mb layer for 28 February through 2 March 1992 from the ECMWF data, while Figs. 3b and 4b illustrate the corresponding mean sea-level pressure field. The PV plots show a steady train of upper-tropospheric potential vorticity anomalies tracking alone remarkably similar paths from Hudson's Bay to the Atlantic via the St. Lawrence River valley, poleward of the jet stream. This pattern, suggestive of near-tropopause baroclinic waves of Whitaker and Barcilon (1992), is evident as far back as 26 February. (A sequence PV anomalies, tracking roughly from the Northwest, is, in fact, evident in most of the data for February and March, 1992, though the

* The original GRIDTOMS data set has 1.25° longitudinal resolution up to 50° latitude, 2.5° resolution from 50° to 70°, and 5° above 70° latitude.

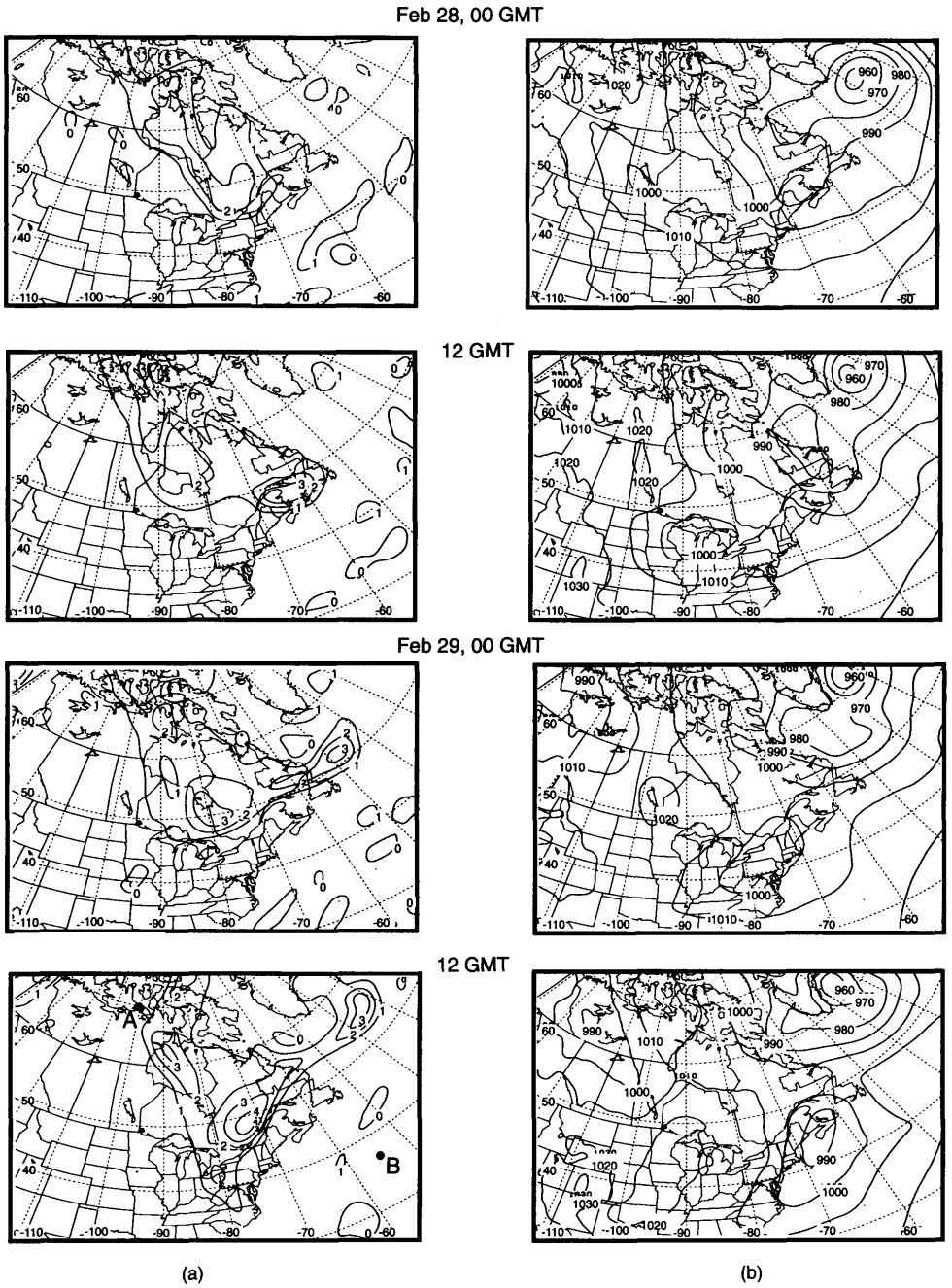

Fig. 3. A series of plots of (a) potential vorticity in the 400 mb to 500 mb layer in "potential vorticity units", (1 PVU = 1 KPa^{-1} s^{-1}) and (b) mean sea-level pressure, in mb, from the ECMWF high-resolution gridded analyzed fields, for 28 and 29 February 1992.

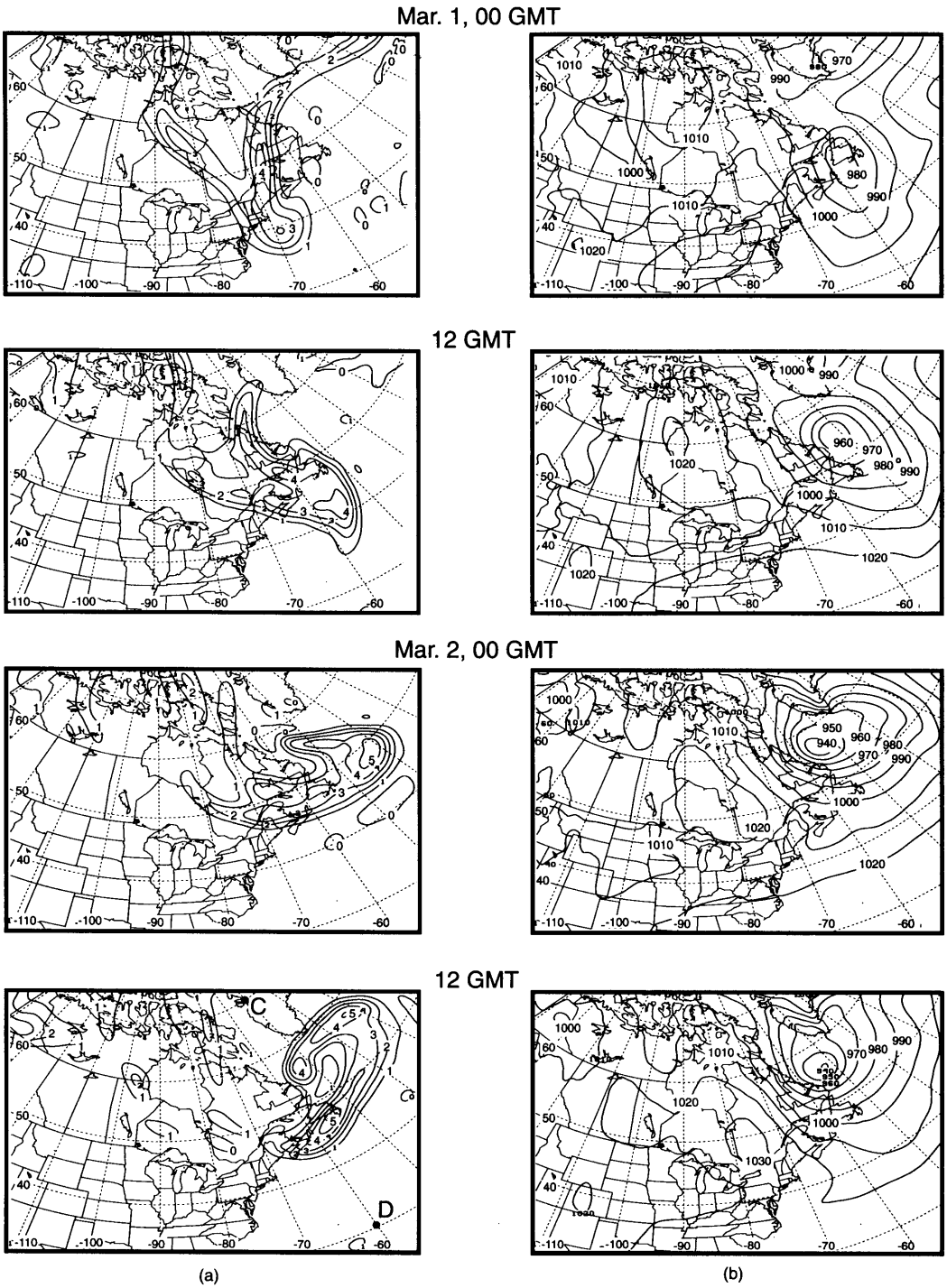

Fig. 4. As above for 1 and 2 March 1992.

exact path shifts considerably, following the jet stream.)

The circumstances responsible for generating these upper-level anomalies are not obvious. In fact, Sanders (1988) found that most cold-season upper-level troughs over North America are produced orographically by the Rocky Mountains, while relatively few develop in the Northern Hudson's Bay region, where the upper-level anomalies associated with this storm appeared to arise. His study does, however, also show a preference for the birth of these features in Northwesterly flow.

The surface low can be traced back to Great Slave Lake at 12:00 GMT on 27 February. Over the next 24 h, it deepened from 1002 mb to 992 mb and traveled Southeast to the Great Lakes region. The primary upper-level vortex involved in this storm was first apparent in the ECMWF data over Northern Hudson's Bay on 27 February. By 00:00 GMT, 29 February, the upper vortex had reached the Southern tip of James Bay and appeared to begin to interact with the surface low, which was over New York State. The upper PV anomaly appeared as two separate maxima in pressure coordinates by 12:00 GMT on 29 February. By 1 March, a 2nd upper-level vortex had arrived in the neighbourhood of the low. It seems likely that this secondary vortex contributed to the intensification of the storm by providing another burst of upper-level forcing. The remarkable subsequent multiple-vortex interactions, visible in Fig. 4, were probably also crucial in determining the characteristics of this storm, most notably its rapid deepening rate. The surface low and upper-level anomalies orbited each other and intensified for another day, culminating in a violent 932 mb cyclone on 2 March. When this maximum depth was reached, the main upper level vortex was directly above the surface low. Examination of similar six hourly plots for 3 March (not shown here) indicates that these vortices remained coupled until 06 GMT on 3 March, at which point the original surface low had filled considerably while another shallow low, apparently associated with the other main upper-level PV maximum, developed east of Greenland.

In addition to the probable forcing by the arrival of "individual" PV anomalies, there also appears to be a larger scale cyclonic "wrapping-up" such as that associated with rapid cyclone deepening by Thorncroft et al. (1993). It is not clear how to separate these two effects.

It is interesting to note that on 29 February, approximately when the rapid development began and 2 days before the maximum depth was reached, the first upper-level anomaly was approximately 1000 km NNW of the surface low. The explosive deepening phase lasted about 2 days. This is reminiscent of the optimal case of "coupling development" in the model of Takayabu (1991). The model is initialized with an upper vortex 1200 km north and 1500 km west of a surface vortex. By day 2 of Takayabu's model simulation, the upper-level vortex was located approximately 1000 km NNW of the surface trough. 12 h later, a 2.5 day explosive development phase began. On day 4 of the simulation, the horizontal positions of the upper and lower vortices were nearly coincident. The maximum surface vorticity was reached on day 5.

Fig. 5 shows cross-sections of potential vorticity and normal wind component, relative humidity and potential temperature at two important stages in the storm's development. The endpoints of the cross-sections are marked on Figs. 3, 4 and 6, though it should be noted that the cross-sections are taken along straight lines on a rectangular projection and so do not correspond to straight lines on the stereographic projections used in these figures. The first pair, Figs. 5a, b, from 12 GMT 29 February, show a tropopause intrusion approaching a surface baroclinic region, consistent with the Type B cyclogenesis paradigm. The 2nd pair, Figs. 5c, d, from 12 GMT 2 March, illustrates the complicated vertical structure of the PV anomalies and upper-level wind field. Notice that both upper PV anomalies visible in the 2 March cross-section have associated cyclonic circulation, but only the more northerly has a clear association with a cyclonic circulation at the surface. Notice that the stratospheric intrusions are also visible in the relative humidity field as regions of anomalously dry air.

These cross-sections also show a weak, low-level PV anomaly near the surface low associated with the cyclonic circulation (this is only obliquely caught in the 2 March section). The high relative humidity of the air comprising the lower anomaly indicates that it originates from diabatic processes in the troposphere. From Fig. 1 it is clear that on 2 March, the large low-level PV anomaly, to the

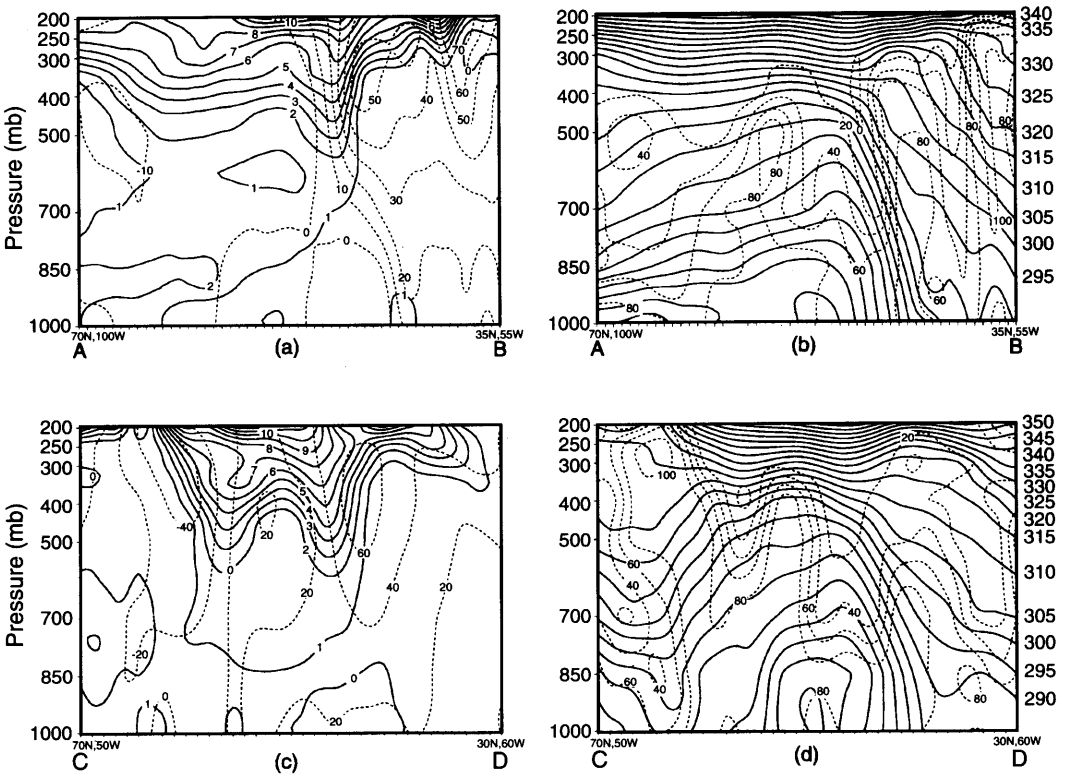

Fig. 5. Cross-sections of (a) potential vorticity (solid, PV units) and normal wind (dashed, m/s) and (b) potential temperature (solid, K) and relative humidity (dashed, %) from the ECMWF analyzed fields at 12 GMT, 29 February. (c) and (d) are as above for 2 March. The cross-sections are taken along lines joining the horizontal positions of the surface low and primary upper-level PV anomaly.

northeast of the surface vortex centre, is in a region of very heavy cloud and so is undoubtably convective in origin.

Fig. 6 shows the evolution of this low-level PV anomaly and its association with a small warm tongue, visible in the 500 mb–1000 mb thickness field. This anomaly gradually intensified throughout the storm's development, though this was somewhat erratic on the 6-h timescale of the ECMWF data. At 12 GMT on 28 February, a closed 1 PVU contour is directly over the Great Lakes region. The surface low, indicated by an "**L**", is located there as well and there is a corresponding small kink visible in the 500 mb–1000 mb thickness field. The explanation for the larger PV anomaly to the southwest, which is prominent only in the 12 GMT data, is not clear. By 12 GMT on 29 February, the $\geqslant 1$ PVU low-level anomaly, low pressure region and kink in the thickness field are over Nova Scotia. On 1 March, they are all of the coast of Labrador, and the low-level PV anomaly has strengthened somewhat. On 2 March, the situation is rather complicated as there is no longer a clear distinction between the surface PV anomaly traveling with the storm and pre-existing anomalies at this latitude. The thickness field shows a clear tongue of warm air curving around into the storm region. Comparison with Figs. 3b, 4b shows that several of the other low-level PV anomalies are associated with surface troughs.

The deformation of the tropopause by the surface low and upper-level frontogenesis can be seen more clearly in Fig. 7a, in which isentropic potential vorticity in the 300 K to 325 K potential tem-

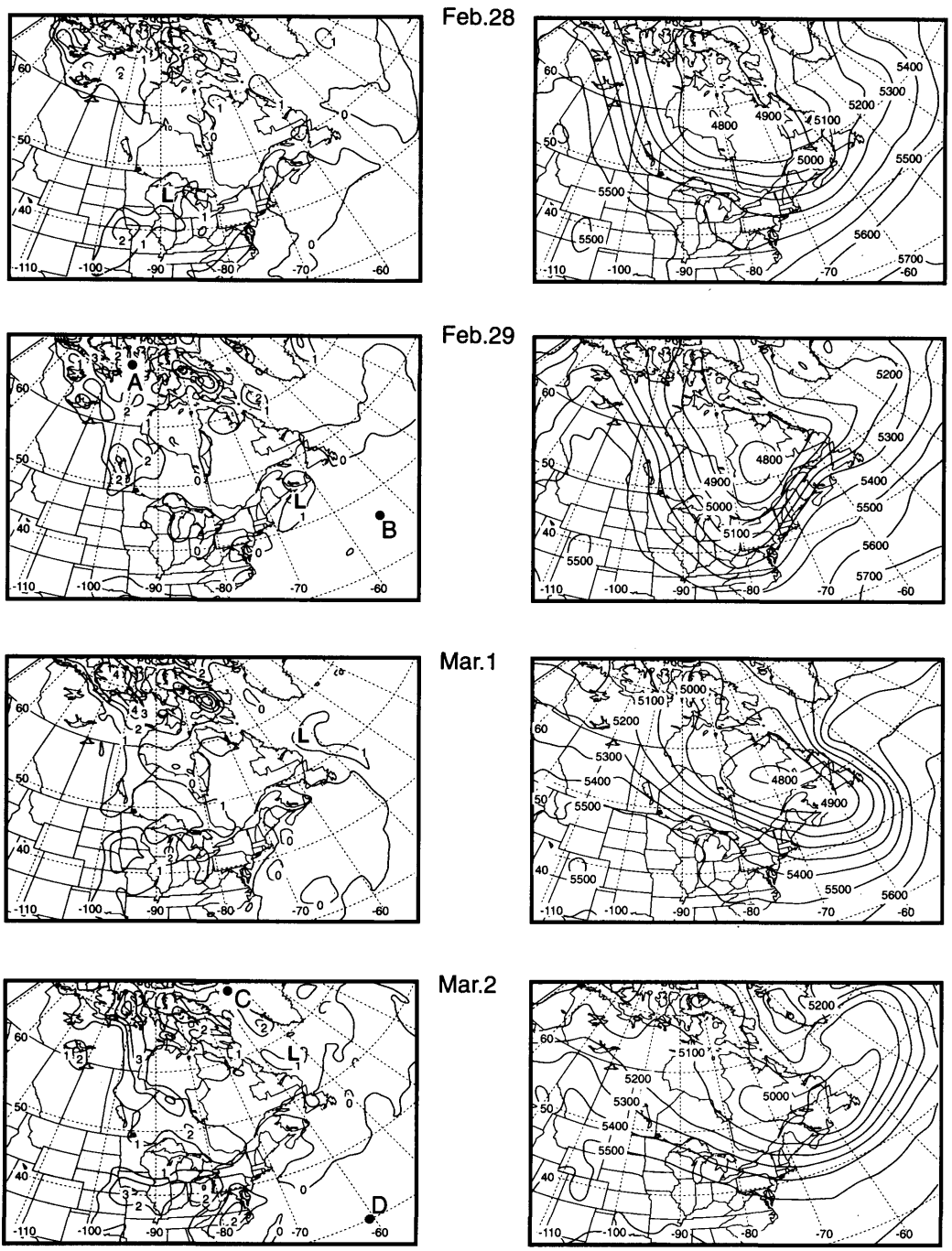

Fig. 6. A series of plots of (a) potential vorticity in the 925 mb to 1000 mb layer (PV units) and (b) 500 mb to 1000 mb thickness (m), from the ECMWF high-resolution gridded analyzed fields at 12 GMT. The location of the surface low is marked with an "L".

Tellus A/47/5:1-23

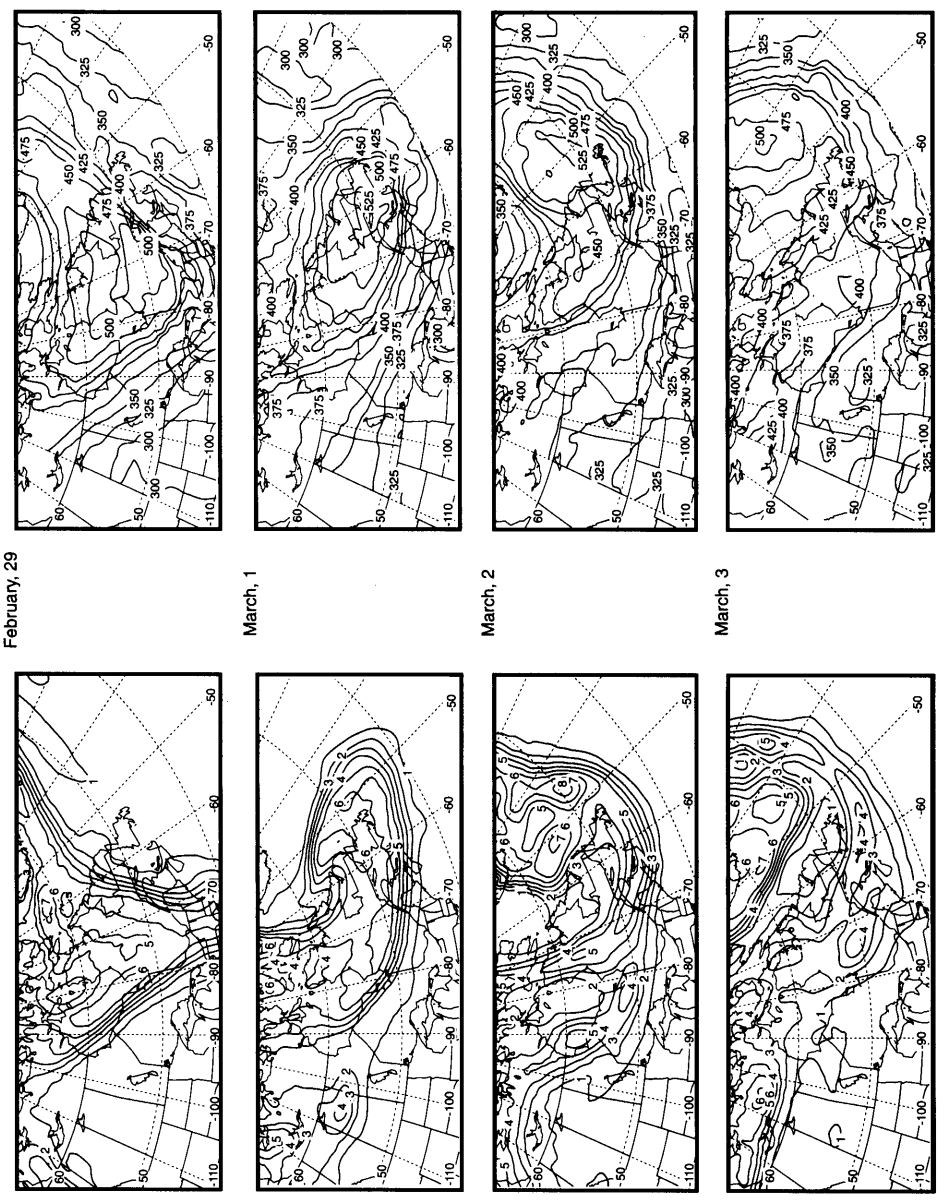

Fig. 7. (a) Isentropic potential vorticity (PV units) and (b) TOMS column ozone data (Dobson units) from the 18 GMT ECMWF data.

perature layer has been contoured for 18 GMT, 29 February through 3 March. The individual PV anomalies are not as apparent in this representation as they were in Figs. 3, 4, because of the curvature of the isentropic surfaces, but the approximate conservation of IPV allows air masses to be tracked more reliably. Also, the polar front is very clear because of the upward slant of the tropospheric potential temperature surfaces with latitude. It is roughly indicated by the region of strong IPV gradient. This figure indicates that the train of PV anomalies propagate along the edge of a wide Southward extrusion of the polar vortex and are not the result of breakup of a narrow streamer, a phenomenon described by Appenzeler and Davies (1992). It is also interesting to note that, as well as showing the warm tongue associated with the surface anomaly, the 500 mb–1000 mb thickness plots also roughly indicate the region of high upper-level potential vorticity. (Compare the low thickness regions of Fig. 6 with the high IPV regions of Fig. 7a, keeping in mind the 6-h time difference between the plots.)

These isentropic potential vorticity maps show the polar front initially wrapping cyclonically around the surface low. During this stage, the anomaly is drawn out meridionally and split. This process, similar to that observed by Bell and Keyser (1993), can be seen more clearly in Figs. 3, 4. The mesoscale local IPV maxima are, at first, simply advected along. The apparent increase of IPV in these anomalies as the storm intensifies is probably, at least partially, a numerical artifact, since it is somewhat erratic on the 6-h time scale. By 3 March, the surface storm dissipates and the composite PV anomaly pinches off from the polar vortex.

4.2. The ozone signature

The increased thickness of the ozone-rich layer of stratospheric air associated with a potential vorticity anomaly should, in principle, be visible in column ozone data of sufficient accuracy and resolution. Total column ozone and column-integrated potential vorticity are well-correlated, especially in winter and string (Allaart et al., 1993). Studies have also shown a positive relationship between column ozone and tropopause pressure (Schubert and Munteanu, 1987; Salby and Callaghan, 1993). In this case, the existence, (and even some of the substructure) of the upper-level anomalies associated with the cyclone, is apparent in both the TOMS and TOVS column ozone data. Fig. 7 compares isentropic potential vorticity (IPV) and TOMS column ozone data for 29 February through 2 March 1992. The qualitative similarity between ozone and IPV contours is striking. It should be noted that the TOMS data is a composite derived from a number of passes of the polar-orbitting satellite at approximately local noon, while the IPV field refers to exactly 18:00 GMT, the nearest synoptic time to local noon in this region. The qualitative correlation between IPV and column ozone is clear.

The plots of Fig. 7 clearly show a large (>525 Dobson units on 1 and 2 March) column ozone maximum propagating into the storm region. The significance of the TOMS ozone anomaly associated with this storm is apparent in comparison with the mean and standard deviation over the Labrador Sea. The average value of TOMS column ozone over the area bounded by 50°N, 60°N, 60°W and 50°W was 405 Dobson units in February and March, 1992, with a standard deviation of 38. It is interesting to note that both the February and March 1992 TOMS data show a broken "ring" of high standard deviation encircling the Labrador Sea, consistent with regions of high upper-level winds and the associated train of PV anomalies leading up to this storm. The March standard deviation data shows a pronounced maximum (>50 Dobson units) in the region of the cyclone on 1 March. If the 1st 3 days of March are removed from the data set, the standard deviation in that area is reduced by at least 10 Dobson units in the region, to values comparable to other areas in the North Atlantic. It is quite remarkable that this one event appears to dominate the ozone variation in the Southern Labrador Sea for the entire month.

Like the PV anomalies in the ECMWF analyzed fields, the TOMS ozone maximum is clearly visible at least as far back as 26 February, though it intensifies as the upper-level PV anomaly interacts with the surface low. In this respect, it is similar to the "President's Day Cyclone", Uccellini et al. (1985). In contrast, however, is the case studied by Reed and Albright (1986) in which subsidence of ozone rich air was observed immediately preceeding explosive development, but no long-lived pre-existing ozone anomaly was evident.

The quantity,

$$\langle \mu_{O_3} \rangle \propto \frac{\Sigma_{O_3}}{p_0}, \tag{4}$$

where Σ_{O_3} is the TOMS column ozone amount and p_0 is the pressure of the 375°K isentropic surface (a material surface near the tropopause) from the ECMWF data closest to the time of the TOMS pass, can be interpreted as an approximate column-averaged ozone mixing-ratio; dividing by p_0 removes the effect of vertical stretching and compression of the air column from the total ozone measurement. To the extent that the air motions are columnar, a reasonable approximation for the stratosphere on this timescale, $\langle \mu_{O_3} \rangle$ can be used as a tracer, yielding further evidence of the origin of ozone anomalies (Salby and Callaghan, 1993). Plots of $\langle \mu_{O_3} \rangle$ support the appearance (Fig. 7) that the ozone anomaly was shed off the polar vortex, while a displacement between the maxima of $\langle \mu_{O_3} \rangle$ and Σ_{O_3} during and after the explosive phase, reflects further intrusion of the tropopause due to interaction with the surface circulation.

Fig. 8 shows the TOVS column ozone data overlayed on an infrared image from 29 February. It clearly shows a column ozone maximum over Lake Ontario, well to the West of the region of cloud, very near to the location of a PV maximum in the ECMWF data. Examination of TOVS data for the period from 27 February to 4 March 1992 shows an almost-perfect one-to-one correspondence between TOVS ozone maxima and locations of PV maxima in the ECMWF data. Unfortunately, the tropopause intrusions indicated by the TOVS column ozone data are not clearly indicated in the HIRS channel 12 (sensitive to upper-tropospheric water vapour content) and TOVS dewpoint retrievals. This merits further investigation. Note that there are no TOVS ozone soundings in extremely cloudy regions and the values in moderately cloudy areas are somewhat suspect. The relevant ozone maxima observed in the TOMS and TOVS data cannot be attributed to the difficulties encountered by both of these

Fig. 8. An AVHRR channel 4 infrared image from 13:05 GMT, 29 February, with TOVS column ozone contours overlayed.

retrievals in cloudy regions since, prior to 1 March they appear in areas of clear sky.

There is clearly some discrepancy between the absolute values of the TOVS and TOMS column ozone data. There are many factors that probably contribute to this, including the smoothing of the gridded TOMS product, retrieval algorithm problems associated with clouds and ice and the time difference between Nimbus 7 and NOAA satellite passes. For the purposes of this study, however, we are only interested in using this data for locating upper-level PV anomalies. The data sets are consistent in this regard.

5. Conclusions

Examination of analyzed fields, satellite images and column ozone data clearly indicates the importance of upper-level forcing in the development of this exceptional storm. Potential vorticity maps for this case, generated from the high-resolution ECMWF analysis, show a relatively stable train of upper-level vortices tracking from the Canadian Arctic for several days preceeding the explosive phase of the storm. The surface low, apparent in the ECMWF data as far back as 12 GMT, 27 February near Great Slave Lake gradually deepened as it tracked Eastward across the continent. A well-defined cyclonic disturbance became visible in AVHRR satellite images on 1 March as one of the upper-level vortices approached a surface low and explosive development began.

The primary upper vortex is also visible in the TOMS column ozone data. The corresponding TOVS data also resolves the fine-scale structure of the upper-level vortices apparent in the ECMWF analysis. This suggests that ozone data might be a useful indicator of mesoscale tropopause structure, especially in regions poorly covered by conventional meteorological data. Remarkably, the arrival of the second PV anomaly appears to have provided additional upper-level support that may have contributed to the exceptionally rapid deepening of the surface low. The complex interactions between the many vortices involved in this storm merit further study. The time and distance scales of this interaction are in good agreement with the optimal parameters for surface development found by Takayabu (1991) in his model study.

Fig. 9 illustrates the above points for this case. The paths of the surface low, the main upper-level vortex, and the TOMS ozone maximum are plotted. The explosive phase of the storm occurred as the upper-level anomaly approached the surface

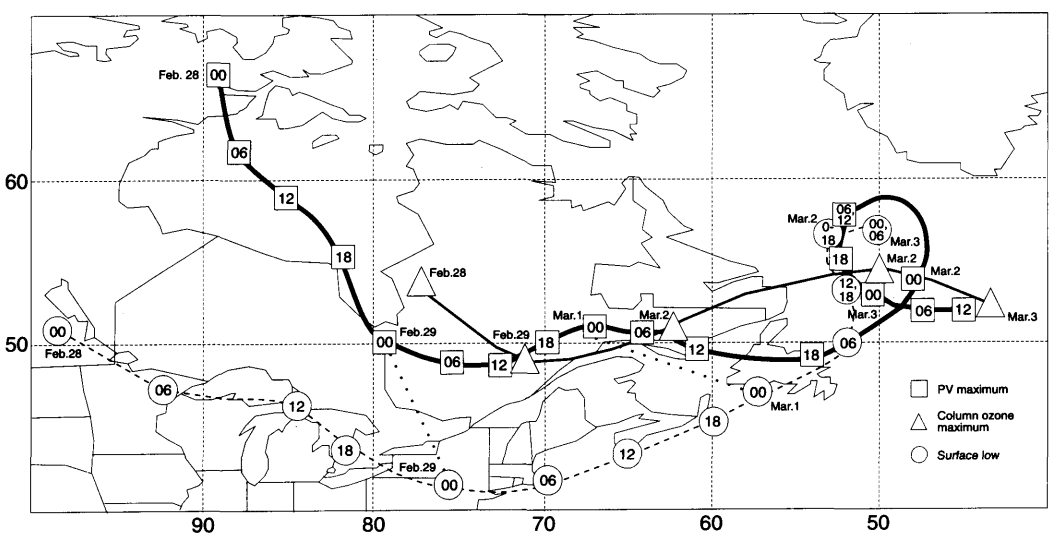

Fig. 9. A map of the paths followed by the main upper-level vortex (squares), the surface low (circles) and the local TOMS ozone maximum (triangles) involved in this storm.

low. The maximum depth of the storm was reached when the horizontal positions of the upper and lower vortices coincided. The TOMS ozone maximum gives a good indication of the location of the main PV anomaly during precyclogenesis and cyclogenesis.

6. Acknowledgments

We would like to thank the NASA Climate Data System Ozone Processing Team for access to the TOMS data, The National Center for Atmospheric Research for the ECMWF data and the Atmospheric Environment Service for the AVHRR and TOVS data for the 2 March case. Vladimir Smirnov wrote the program for interpolating pressure-level data to isentropic levels. We are also grateful for helpful discussions with John Gyakum and Ron Stewart.

Support for this research has come from the Japan-Canada Fund, the Atmospheric Environment Service and the Natural Sciences and Engineering Research Council of Canada.

REFERENCES

Allaart, M. A. F., Kelder, H. and Hijboer, L. C. 1993. On the relation between ozone and potential vorticity. *Geophys. Res. Lett.* **20**, 811–814.

Appenzeler, C. and Davies, H. C. 1992. Structure of stratospheric intrusions into the troposphere. *Nature* **358**, 570–572.

Bell, G. D. and Keyser, D. 1993. Shear and curvature vorticity and potential-vorticity interchanges: interpretation and application to a cutoff cyclone event. *Mon. Wea. Rev.* **121**, 76–102.

Bleck, R. 1973. Numerical forecasting experiments based on the conservation of potential vorticity on isentropic surfaces. *J. Appl. Mateor.* **12**, 737–752.

Bretherton, F. P. 1966. Critical layer instability in baroclinic flows. *Q. J. R. Meteorol. Soc.* **92**, 325–334.

Danielson, E. F. 1968. Stratospheric-tropospheric exchange based on ozone and potential vorticity. *J. Atmos. Sci.* **25**, 502–518.

ECMWF 1992. *The description of the ECMWF/WCRP Level III-A global atmospheric data archive.* Available from the European Centre for Medium Range Weather Forecasts.

Gyakum, J. R. and Barker, E. S. 1988. A case study of explosive subsynoptic-scale cyclogenesis. *Mon. Wea. Rev.* **116**, 2225–2253.

Hoskins, B. J., McIntyre, M. E. and Robertson, A. W. 1985. On the use and significance of potential vorticity maps. *Q. J. R. Meteorol. Soc.* **111**, 877–946.

Keyser, D. and Shapiro, M. A. 1985. A review of the structure and dynamics of upper-level frontal zones. *Mon. Wea. Rev.* **114**, 452–499.

Kleinschmidt, E. 1950a. Über Aufbau und Entstehung von Zyclonen (1. Teil). *Met. Runds.* **3**, 1–6.

Kleinschmidt, E. 1950b. Über Aufbau und Entstehung von Zyclonen (2. Teil). *Met. Runds.* **3**, 54–61.

Kleinschmidt, E. 1951. Über Aufbau und Entstehung von Zyclonen (3. Teil). *Met. Runds.* **4**, 89–96.

McPeters, R., Arlin, J., Krueger, P., Bhartia, J., Oaks, A., Ziuddin, A., Cebula, R., Schlesinger, B., Swissler, T., Taylor, S., Torres, O. and Wellemeyer, C. 1993. Nimbus-7 Total Ozone Mapping Spectrometer (TOMS) Data Products User's Guide. *NASA Reference Publication* **1323**.

Mote, P. W., Holton, J. R. and Wallace, J. M. 1991. Variability in total ozone associated with baroclinic waves. *J. Atmos. Sci.* **48**, 1900–1903.

Petterssen, S. and Smebye, S. J. 1971. On the development of extratropical storms. *Quart. J. Roy. Meteor. Soc.* **97**, 457–482.

Reed, R. J. 1950. The role of vertical motions in ozone-weather relationships. *J. Meteor.* **7**, 263–267.

Reed, R. J. and Albright, M. D. 1986. A case study of explosive cyclogenesis in the eastern pacific. *Mon. Wea. Rev.* **114**, 2297–2319.

Reed, R. J., Simmons, A. J., Albright, M. D. and Undén, P. 1988. The role of latent heat release in explosive cyclogenesis: three examples based on ECMWF operational forecasts. *Wea. Forecasting* **3**, 217–229.

Rodgers, E. B., Stout, J., Steranka, J. and Chang, S. 1990. Tropical cyclone-upper atmosphere interaction as inferred from satellite total ozone observations. *J. App. Meteor.* **29**, 934–954.

Roebber, P. J. 1984. Statistical analysis and updated climatology of explosive cyclones. *Mon. Wea. Rev.* **112**, 1577–1589.

Salby, M. L. and Callaghan, P. F. 1993. Fluctuations of total ozone and their relationship to stratospheric air motions. *J. Geophys. Res.* **98**, 2715–2727.

Sanders, F. 1980. Explosive cyclogenesis in the West-central North Atlantic Ocean, 1981–1984. Part I: composite structure and mean behavior. *Mon. Wea. Rev.* **114**, 1589–1606.

Sanders, F. and Gyakum, J. 1980. Synoptic-dynamic climatology of the "bomb", *Mon. Wea. Rev.* **108**, 1589–1606.

Sanders, F. 1988. Life history of mobile troughs in the upper westerlies. *Mon. Wea. Rev.* **116**, 2629–2648.

Schubert, S. D. and Munteanu, M. 1988. An analysis of

tropopause pressure and total ozone correlations. *Mon. Wea. Rev.* **116**, 569–582.

Sechrist, F. S., Peterssen, R. A., Brill, K. F., Krueger, A. J. and Uccellini, L. W. 1986. Ozone, jet streams and severe weather. *Second Conference on Satellite meteorology/remote sensing and applications*, preprint volume, 388–392. American Meteorological Society.

Shapiro, M. A., Krueger, A. J. and Kennedy, P. J. 1982. Nowcasting the position and intensity of jet streams using a satellite-borne total ozone mapping spectrometer. *Nowcasting*, K. A. Browning (ed.), Academic Press, 137–145.

Smith, W. L., Woolf, H. M., Hayden, C. M. and Schreiner, A. J. 1985. The simultaneous retrieval export package. *The Technical Proceedings of the 2nd International TOVS Study Conference*, Igls, Austria (ed. W. P. Menzel). Cooperative Institute for Meteorological Satellite Studies, Madison, Wisconsin.

Takayabu, I. 1991. Coupling development. An efficient mechanism for the development of extratropical cyclones. *J. Meteor. Soc. Japan* **69**, 609–628.

Thorncroft, C. D., Hoskins, B. J. and McIntyre, M. E. 1993. Two paradigms of baroclinic-wave life-cycle behaviour. *Q. J. R. Meteorol. Soc.* **119**, 17–55.

Tosi, E., Smith, R. B. and Bradford, M. L. 1987. Aerial observations of stratospheric descent in a Gulf of Genoa cyclone. *Meteorol. Atmos. Phys.* **36**, 141–160.

Uccellini, L. W. 1990. Processes contributing to the rapid development of extratropical cyclones. *Extratropical Cyclones: The Erik Palmén memorial volume.* (ed. C. Newton and E. H. Holopainen), pp. 81–105.

Uccellini, L. W., Keyser, D. and Brill, K. F. 1985. The Presidents' Day cyclone of 18–19 February 1979: Influence of upstream trough amplification and associated tropopause folding on rapid cyclogenesis. *Mon. Wea. Rev.* **113**, 962–987.

Whitaker, J. and Barcilon, A. 1992. Genesis of mobile troughs in the upper Westerlies. *J. Atmos. Sci.* **49**, 2097–2107.

Whitaker, J. S., Uccellini, L. W. and Brill, K. F. 1988. A model-based diagnostic study of the rapid development phase of the Presidents' Day cyclone. *Mon. Wea. Rev.* **116**, 2337–2365.